







RESEARCH ARTICLE

A versatile look-up algorithm for mapping pH values and magnesium ion content using ^{31}P MRSI

Vanessa L. Franke¹  | Johannes Breitling¹  | Philip S. Boyd¹  |
 Antoine Feignier¹ | Renate Bangert¹ | Nina Weckesser² |
 Heinz-Peter Schlemmer^{2,3}  | Mark E. Ladd^{1,3,4}  | Peter Bachert^{1,4} |
 Daniel Paech^{2,5}  | Andreas Korzowski¹ 

¹Division of Medical Physics in Radiology, German Cancer Research Center (DKFZ), Heidelberg, Germany

²Division of Radiology, German Cancer Research Center (DKFZ), Heidelberg, Germany

³Faculty of Medicine, Heidelberg University, Heidelberg, Germany

⁴Faculty of Physics and Astronomy, Heidelberg University, Heidelberg, Germany

⁵Division of Neuroradiology, University Hospital Bonn, Bonn, Germany

Correspondence

Andreas Korzowski, Division of Medical Physics in Radiology, German Cancer Research Center (DKFZ), Im Neuenheimer Feld 223, 69120 Heidelberg, Germany.
 Email: a.korzowski@dkfz.de

[Correction added on 19 February 2024, after first online publication: The Data Availability Statement was added in this version.]

^{31}P MRSI allows for the non-invasive mapping of pH and magnesium ion content (Mg) in vivo, by translating the chemical shifts of inorganic phosphate and adenosine-5'-triphosphate (ATP) to pH and Mg via suitable calibration equations, such as the modified Henderson-Hasselbalch equation. However, the required constants in these calibration equations are typically only determined for physiological conditions, posing a particular challenge for their application to diseased tissue, where the biochemical conditions might change manyfold. In this article, we propose a multi-parametric look-up algorithm aiming at the condition-independent determination of pH and Mg by employing multiple quantifiable ^{31}P spectral properties simultaneously. To generate entries for an initial look-up table, measurements from 114 model solutions prepared with varying chemical properties were made at 9.4 T. The number of look-up table entries was increased by inter- and extrapolation using a multi-dimensional function developed based on the Hill equation. The assignment of biochemical parameters, that is, pH and Mg, is realized using probability distributions incorporating specific measurement uncertainties on the quantified spectral parameters, allowing for an estimation of most plausible output values. As proof of concept, we applied a version of the look-up algorithm employing only the chemical shifts of γ - and β -ATP for the determination of pH and Mg to in vivo 3D ^{31}P MRSI data acquired at 7 T from (i) the lower leg muscles of healthy volunteers and (ii) the brains of patients with glioblastoma. The resulting volumetric maps showed plausible values for pH and Mg, partly revealing differences from maps generated using the conventional calibration equations.

KEYWORDS

^{31}P MRS, ^{31}P MRSI, magnesium, magnesium ion concentration, pH, pH imaging

Abbreviations: ATP, adenosine-5'-triphosphate; DPG, 2,3-diphosphoglycerate; eP_i , extracellular P_i ; GPC, glycerophosphocholine; Mg, magnesium ion content; MPL, mobile phospholipid; NAD(H), nicotinamide adenine dinucleotide; NOE, nuclear Overhauser effect; PC, phosphocholine; PCr, phosphocreatine; PE, phosphoethanolamine; P_i , inorganic phosphate; SNR, signal-to-noise ratio; UDPG, uridine diphosphoglucose.

This is an open access article under the terms of the [Creative Commons Attribution-NonCommercial](https://creativecommons.org/licenses/by-nc/4.0/) License, which permits use, distribution and reproduction in any medium, provided the original work is properly cited and is not used for commercial purposes.

© 2024 The Authors. *NMR in Biomedicine* published by John Wiley & Sons Ltd.

1 | INTRODUCTION

The pH value and the magnesium ion content (Mg) play key roles in numerous metabolic and enzymatic processes of living tissue, and might be altered under pathophysiological conditions. Therefore, the assessment of pH and Mg are of great interest in biomedical research, as they can be potentially used as biomarkers in different pathologies, such as cancer,^{1–6} diabetes,⁷ and also muscular,⁸ psychiatric,^{9,10} and neurodegenerative diseases.^{11,12}

A non-invasive method to determine pH and Mg in vivo is phosphorus (³¹P) MRS. The use of MRSI methods further allows for two- or three-dimensional imaging of pH and Mg in the entire investigated volume, which is of great value, as, for example, it enables the comparison of healthy and diseased tissue from a single measurement.

The determination of pH and Mg by means of ³¹P MRS(I) is conventionally done via suitable calibration equations relating the measured chemical shifts of specific ³¹P metabolites to the biochemical parameters, that is, pH and Mg. For the case of pH, typically, a modified form of the Henderson–Hasselbalch equation employing the chemical shift difference between inorganic phosphate (P_i) and phosphocreatine (PCr) is used.^{13,14} The determination of the free magnesium ion concentration is conventionally done by using the chemical shift difference between the α - and β -resonances of adenosine-5'-triphosphate (ATP),^{15,16} or alternatively between β -ATP and PCr.¹⁷

However, the required constants in these calibration equations are typically only characterized for certain sets of physiological conditions—for example, for a specific ionic strength. This poses a particular challenge for the application of these calibration equations to pathophysiological conditions^{18–21}—for example, in tumor tissue, where the biochemical conditions can be altered substantially.²² Hence, the reliability of the conventional methods for the determination of pH and Mg in pathologies might be hampered.

To overcome this challenge, we propose a look-up algorithm for the determination of pH and Mg by means of ³¹P MRS, which is applicable under varying chemical environments. Applying the implemented algorithm to quantified ³¹P MRSI datasets allows for the volumetric mapping of pH and Mg.

The basic idea of the proposed look-up algorithm is to make use of multiple properties of a ³¹P spectrum to determine the underlying biochemical parameters. As a first proof of concept, the proposed look-up algorithm is implemented in such a way that pH and Mg can be determined for different ionic strengths by using only the chemical shifts of the ATP resonances.

In this article, we want to demonstrate the principal idea of this multi-parametric look-up algorithm. To this end, we (i) describe the generation of the look-up table elements based on measurements in a model solution, (ii) explain the implementation of the look-up algorithm itself, and (iii) show the first results of the application of the implemented algorithm to in vivo ³¹P MRSI data.

2 | EXPERIMENTAL

2.1 | Basic concept of the look-up-based algorithm

The basic idea of the look-up algorithm is to assign the measured chemical shifts of ATP, that is, (δ_γ , δ_α , δ_β), to the unknown parameters (pH, Mg, Ion). Hereby, the parameter Ion represents a unitless surrogate for the total ionic strength without breaking down the individual ionic contributions. To this end, a look-up table was generated, composed of the measured chemical shifts of γ -, α - and β -ATP acquired in suitable model solutions, which will be described in Section 2.2.

Based on this created look-up table, the implemented search algorithm can assign possible solution triples (pH, Mg, Ion) to the input measured chemical shift triple (δ_γ , δ_α , δ_β) (cf. Figure 1).

2.2 | Acquisition of look-up table elements

The entries of the look-up table, that is, the chemical shifts (δ_γ , δ_α , δ_β), are determined from ³¹P spectra acquired in model solutions prepared with different pH, Mg and ionic compositions. In total, 114 different model solutions were prepared and used to fill 2 mL Eppendorf tubes. All model solutions contained 5 mM of P_i, PCr, and ATP. Due to the use of sodium-based salts, all model solutions had a sodium concentration of 29 mM. A list of the used chemicals can be found in Supporting Information S1. The variation of the parameter Ion was realized by adding different amounts of potassium chloride (KCl). An Ion value of 1 corresponds to a KCl concentration of 200 mM. Five different model solution sets with varying values for (pH, Mg, Ion) were prepared (cf. Table 1).

All model solutions were measured on either the same day or 1 day after the preparation, at a 9.4 T Bruker small animal scanner using a double-resonant ³¹P–¹H volume resonator with an inner diameter of 35 mm. For each measurement, the 2 mL Eppendorf tube containing the model solution was placed and fixed into a self-built phantom-mount, which was filled with preheated water to decrease susceptibility changes at the edges of the Eppendorf tube in order to provide improved shimming conditions. The self-built phantom-mount had a volume of 50 mL and

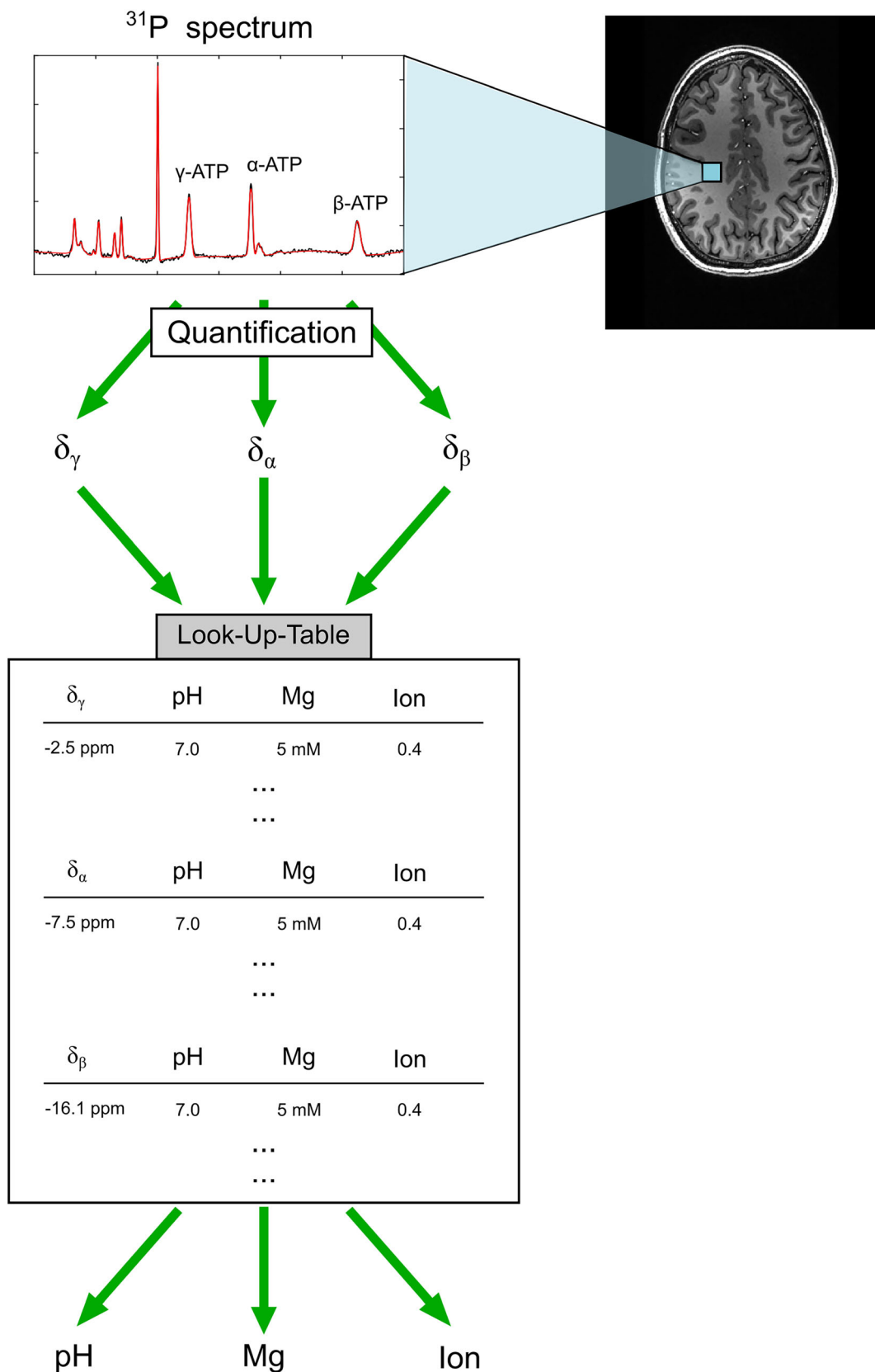


FIGURE 1 Schematic representation of the basic concept of the developed look-up approach. The basic idea is to make use of multiple parameters of a quantified ³¹P spectrum for determination of the underlying biochemical parameters. As proof of concept, a look-up algorithm was implemented, which aims at the assignment of the quantified ATP chemical shifts, that is, (δ_γ , δ_α , δ_β), to the unknown parameters (pH, Mg, Ion).

TABLE 1 Chemical composition of prepared and measured sets of model solutions for generation of the look-up table. The target pH values and magnesium ion concentrations as well as the ionic strengths, given as the unitless parameter *Ion*, are shown. An *Ion* value of 1 corresponds to the addition of 200 mM of KCl. All model solutions had metabolite concentrations of 5 mM each of PCr, P_i , and ATP. Due to the use of sodium-based salts, all model solutions had a sodium concentration of 29 mM (cf. Supporting Information S1).

Set	pH	[Mg ²⁺] (mM)	<i>Ion</i>
1	6.8, 7.0, 7.2, 7.4	0, 1.25, 2.5, 3.75, 5, 10	0.145
2	6.8, 7.0, 7.2, 7.4	0, 1.25, 2.5, 3.75, 5, 10	0.6
3	6.8, 7.0, 7.2, 7.4	0, 1.25, 2.5, 3.75, 5, 10	0.8
4	7.0, 7.4	0.625, 2.5	0, 0.25, 0.375, 0.5, 0.75, 1
5	6.8, 7.4	0, 5, 10	0, 0.5, 1

was additionally equipped with a thermometer enabling to track the temperature of the water in the outer vial. During the acquisition of the ³¹P spectra, the temperature was stabilized at about 37°C by using the heating system of the small animal bed. The mean temperature during the acquisition across all 114 measurements was (37.1 ± 0.3) °C. For the acquisition of the ³¹P spectra, a standard ³¹P free induction decay (FID) sequence was used with the following parameters: sinc-shaped excitation pulse with a flip angle of 45°, bandwidth = 10 kHz, T_R = 0.3 s, 1024 excitations. The total measurement time per acquired spectrum was 5 min 7 s.

No post-processing of data—for example, time domain filtering or zero-filling—was applied prior to quantification. The quantification of the acquired ³¹P spectra was done using a custom-made implementation of the AMARES algorithm²³ for MATLAB.¹ All contained metabolites, that is, P_i , PCr, and ATP, were quantified with Lorentzian lineshapes. ATP was modeled with the corresponding multiplet structure, that is, doublets for γ - and α -ATP, triplet for β -ATP. More details of the applied fitting models can be found in Tables S4.1 and S4.2 in the Supporting Information. The quantified chemical shifts (δ_γ , δ_α , δ_β) relative to PCr were assigned to the corresponding prepared values for (pH, Mg, *Ion*). For δ_γ and δ_α the mean frequency of the two quantified peaks within the doublets was used, for δ_β the frequency of the quantified central resonance.

Based on the measured temperature of the model solution during the acquisition of the spectrum, the exact value for the assigned pH value in the look-up table was corrected for temperature deviations from the target temperature of 37 °C. This temperature correction was implemented based on preliminary experiments on the pH(*T*) dependence of the prepared model solution (for further information see Chapter 4.4.3 in Reference 24).

2.3 | Implementation of the look-up algorithm

The limited number of acquired entries for the look-up table, that is, the quantified chemical shifts from the 114 model solutions, was extended by inter- and extrapolating the measured chemical shifts (δ_γ , δ_α , δ_β) using a model function developed based on the Hill equation. The full description of the used model function $\delta_i^{\text{model}}(\text{pH}, \text{Mg}, \text{Ion})$ can be found in Supporting Information S2. The extrapolation of values for the magnesium ion concentration to a range larger than experimentally covered (extrapolation to up to [Mg²⁺] = 25 mM) is assumed to be justified, because the $\delta(\text{Mg})$ dependence already starts to plateau at around [Mg²⁺] = 10 mM (cf. Figure S2).

For the inter- and extrapolation of the multi-dimensional value space, the following sampling grids were chosen: pH = [6.7:0.01:7.4]; Mg = [0:0.1:25] mM; *Ion* = [0:0.025:1]. Hence, the interpolated look-up table has 833 571 entries. Note that, in the current form of the look-up algorithm, the final parameter assignment is done on these interpolated entries.

In principle, the assignment of a measured chemical shift δ_i^{meas} , $i \in \{\gamma, \alpha, \beta\}$ to possible combinations of the underlying biochemical parameters (pH, Mg, *Ion*) is given by the model functions $\delta_i^{\text{model}}(\text{pH}, \text{Mg}, \text{Ion})$. However, the non-linearity of the model functions makes their inversion challenging. Therefore, a search algorithm is implemented, which finds possible solution triples (pH, Mg, *Ion*) for a given measured chemical shift δ_i^{meas} in a numerical manner.

For each pair of Mg and *Ion* values, that is, (Mg_{*k*}, *Ion*_{*k*}) with *k* being one point in the two-dimensional (Mg–*Ion*) value space of the sampling grid (cf. Figure 2), the pH value is determined, which corresponds to the measured chemical shift δ_i^{meas} , defined by the model function $\delta_i^{\text{model}}(\text{pH})|_{\text{Mg}_k, \text{Ion}_k}$. This assignment yields one pH value pH_{*k*} for each value pair (Mg_{*k*}, *Ion*_{*k*}), that is, $(\delta_i^{\text{meas}}) \rightarrow (\text{pH}_k, \text{Mg}_k, \text{Ion}_k)$. The assignment of a measured chemical shift to possible solution triples (pH_{*k*}, Mg_{*k*}, *Ion*_{*k*}) is done separately for γ -, α - and β -ATP based on the corresponding model function $\delta_i^{\text{model}}(\text{pH}, \text{Mg}, \text{Ion})$, yielding the solution sets (pH_{*k*}, Mg_{*k*}, *Ion*_{*k*}) _{γ} , (pH_{*k*}, Mg_{*k*}, *Ion*_{*k*}) _{α} and (pH_{*k*}, Mg_{*k*}, *Ion*_{*k*}) _{β} . Because the measured chemical shifts δ_γ , δ_α , and δ_β result from the same ³¹P spectrum, and therefore correspond to the same chemical environment, that is, the same values for (pH, Mg, *Ion*), only the solution triple for which the condition

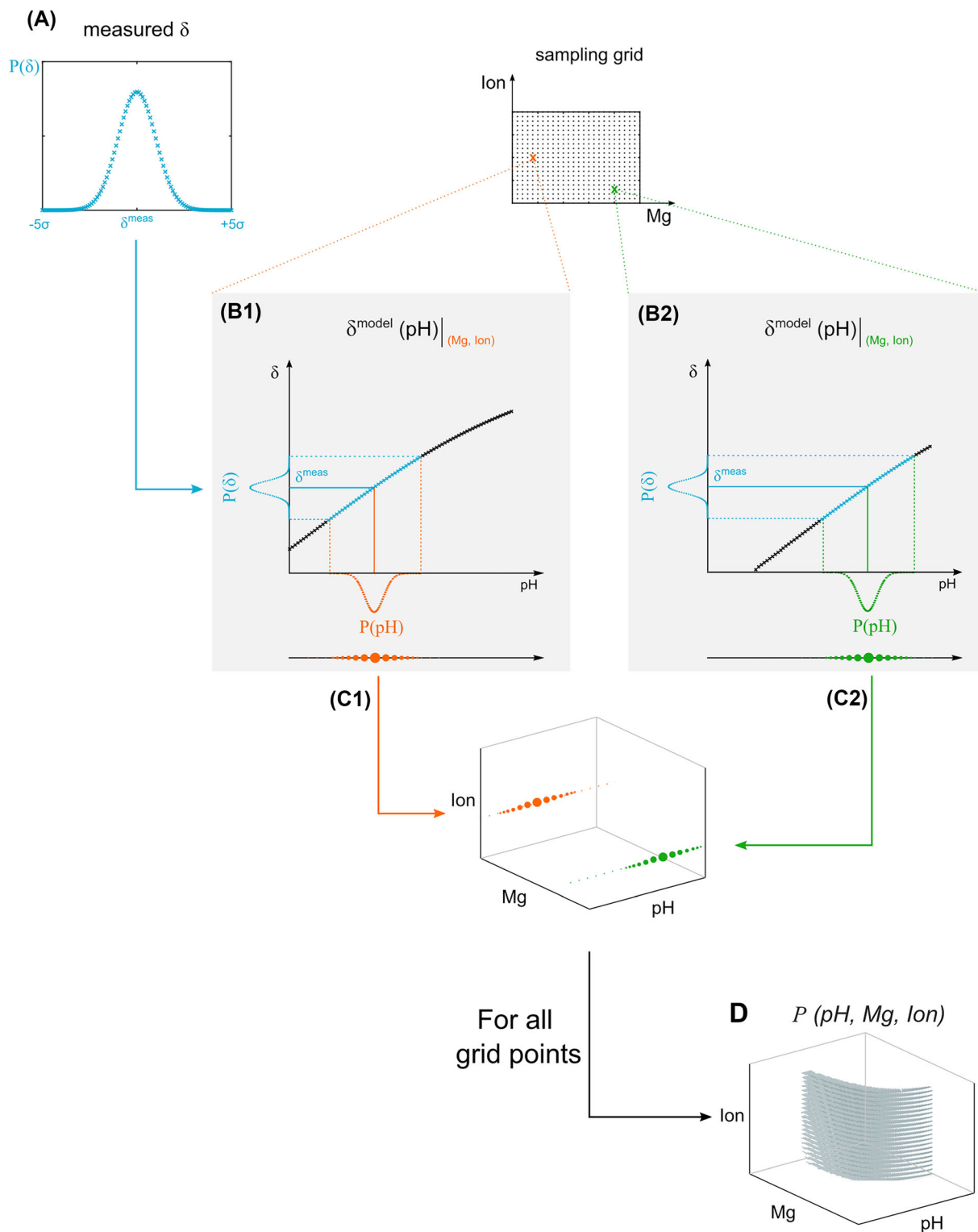


FIGURE 2 Schematic representation of the workflow for the calculation of the multi-dimensional probability distributions $P(\text{pH}, \text{Mg}, \text{Ion})$. A, The error margin of the measured chemical shift (δ^{meas}) is determined by a pre-defined chemical shift range $\Delta\delta^{\text{meas}}$, which is weighted by a Gaussian distribution with a specific width σ , approximated from the frequency precision of the used fitting model. B1, B2, For each point in the sampling grid defined by the subspace $(\text{Mg}-\text{Ion})$, the probability distribution $P(\delta^{\text{meas}} \pm 5\sigma)$ is projected onto the pH axis, which is defined by the model function $\delta^{\text{model}}(\text{pH})|_{(\text{Mg}_k, \text{Ion}_k)}$. C1, C2, The probability distribution $P(\text{pH})$ is interpolated and assigned to the corresponding point in the sampling grid $(\text{Mg}-\text{Ion})$. In the illustration, the dot size corresponds to the value for $P(\text{pH})$. D, This assignment is done for all grid points $(\text{Mg}_k, \text{Ion}_k)$, yielding a multi-dimensional probability distribution $P(\text{pH}, \text{Mg}, \text{Ion})$, which assigns each point in the grid $(\text{pH}-\text{Mg}-\text{Ion})$ a specific probability. Source: Figure is taken and adapted with permission from Reference 24.

$$(\text{pH}_k, \text{Mg}_k, \text{lon}_k)_\gamma = (\text{pH}_k, \text{Mg}_k, \text{lon}_k)_\alpha = (\text{pH}_k, \text{Mg}_k, \text{lon}_k)_\beta \quad (1)$$

holds is assumed to be the correct solution triple. However, under realistic conditions, the constraint in Equation 1 cannot be found exactly due to measurement uncertainties, that is, uncertainties on the quantified chemical shift, as well as uncertainties of the developed model functions. Therefore, the assignment as described before was extended by also incorporating a realistic error margin on the obtained chemical shifts. Hence, the assignment of possible solution triples $(\text{pH}_k, \text{Mg}_k, \text{lon}_k)$ as described above is done not only for δ^{meas} , but for each point in the range $\delta = (\delta^{\text{meas}} \pm \Delta\delta^{\text{meas}})$. The error margin $\Delta\delta^{\text{meas}}$ is determined by a pre-defined chemical shift range, which is weighted according to a Gaussian distribution with a width of σ (Figure 2A). In this study, σ is defined based on the approximated frequency precision of the fitting model used. Note that other metrics for $\Delta\delta^{\text{meas}}$ are also possible (cf. Section 4.3).

The assignment $\delta \rightarrow (\text{pH}, \text{Mg}, \text{lon})$ is realized in the following steps:

1. For each element in $\delta = (\delta^{\text{meas}} \pm 5\sigma)$, and for each point $(\text{Mg}_k, \text{lon}_k)$, the pH value is determined for which the chemical shift defined by $\delta_i^{\text{model}}(\text{pH})|_{\text{Mg}_k, \text{lon}_k}$ is closest to the measured chemical shift δ^{meas} (Figure 2B1, B2). This means that the probability distribution $P(\delta)$ is projected onto the pH axis defined by δ^{model} . Note that the probability distribution $P(\text{pH})$ is not a Gaussian distribution due to the non-linearity of the model function.
2. The probability distribution $P(\text{pH})$ is interpolated using a Hermite spline and assigned to the corresponding point $(\text{Mg}_k, \text{lon}_k)$ in the grid (Figure 2C1, C2).
3. Repeating this projection for each point in the sampling grid (Mg-lon) yields the final probability distribution $P(\text{pH}, \text{Mg}, \text{lon})$ (Figure 2D), assigning each point in the grid a specific probability to which the input chemical shift δ^{meas} corresponds.
4. $P(\text{pH}, \text{Mg}, \text{lon})$ is normalized.

The probability distributions $P(\text{pH}, \text{Mg}, \text{lon})$ are determined for the chemical shifts of γ -, α -, and β -ATP, yielding $P(\text{pH}, \text{Mg}, \text{lon})_\gamma$, $P(\text{pH}, \text{Mg}, \text{lon})_\alpha$, and $P(\text{pH}, \text{Mg}, \text{lon})_\beta$ (cf. Figure 3). Condition (1) yielding the “correct” solution triple $(\text{pH}, \text{Mg}, \text{lon})$ is realized by calculating the joint probability distribution P_{joint} by multiplying $P(\text{pH}, \text{Mg}, \text{lon})_i$, $i \in (\gamma, \alpha, \beta)$. The final output values of the look-up algorithm $(\text{pH}_{\text{out}}, \text{Mg}_{\text{out}}, \text{lon}_{\text{out}})$ are determined as the weighted mean values of all possible solutions:

$$\text{pH}_{\text{out}} = \frac{\sum_{i_{\text{grid}}=1}^{N_{\text{grid}}} (p_{i_{\text{grid}}}^{\text{joint}} \text{pH}_{i_{\text{grid}}})}{\sum_{i_{\text{grid}}=1}^{N_{\text{grid}}} p_{i_{\text{grid}}}^{\text{joint}}} \quad (2)$$

$$\text{Mg}_{\text{out}} = \frac{\sum_{i_{\text{grid}}=1}^{N_{\text{grid}}} (p_{i_{\text{grid}}}^{\text{joint}} \text{Mg}_{i_{\text{grid}}})}{\sum_{i_{\text{grid}}=1}^{N_{\text{grid}}} p_{i_{\text{grid}}}^{\text{joint}}} \quad (3)$$

$$\text{lon}_{\text{out}} = \frac{\sum_{i_{\text{grid}}=1}^{N_{\text{grid}}} (p_{i_{\text{grid}}}^{\text{joint}} \text{lon}_{i_{\text{grid}}})}{\sum_{i_{\text{grid}}=1}^{N_{\text{grid}}} p_{i_{\text{grid}}}^{\text{joint}}} \quad (4)$$

2.4 | Application to in vivo ^{31}P MRSI data

The implemented look-up algorithm was applied to various ^{31}P MRSI datasets acquired in vivo, that is, three datasets acquired in the human lower leg muscle of healthy volunteers, and three datasets acquired in the human brain of patients with glioblastoma. All examinations were approved by the local ethics committee of the Medical Faculty of Heidelberg University, and written informed consent was received from all subjects. All MRSI datasets were acquired at a field strength of $B_0 = 7 \text{ T}$ (MAGNETOM 7 T, Siemens Healthineers). For shimming, a second order vendor-provided 3D gradient echo fieldmap using the unsuppressed water resonance was used. Minimum reporting standards for this study can be found in Supporting Information S6.

Input

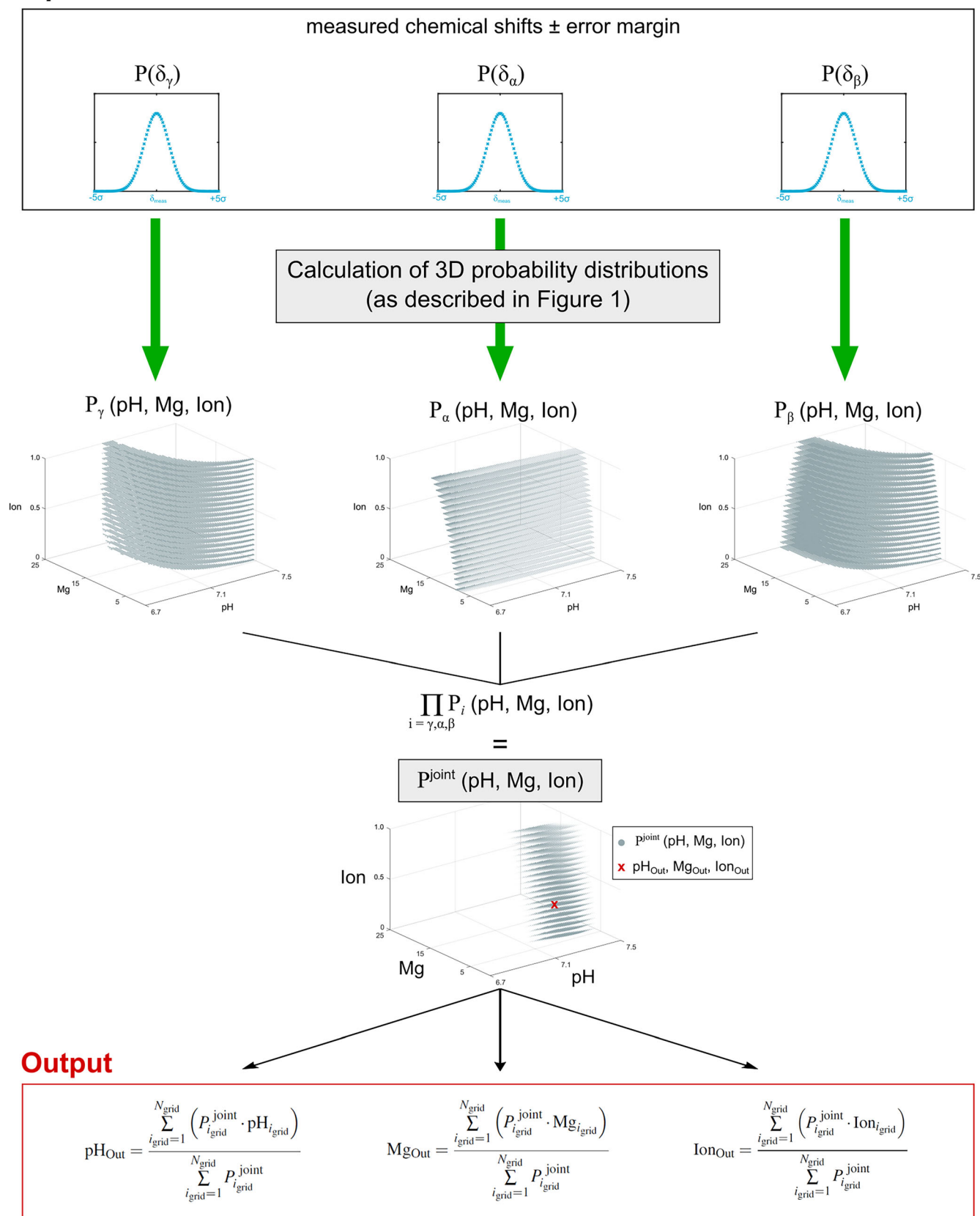


FIGURE 3 Legend on next page.

FIGURE 3 Schematic representation of the workflow for the determination of pH_{Out} , Mg_{Out} , and Ion_{Out} using the presented look-up algorithm. For the measured chemical shifts $\delta_{\gamma}^{\text{meas}}$, $\delta_{\alpha}^{\text{meas}}$, and $\delta_{\beta}^{\text{meas}}$, and their error margin, the probability distributions $P_{\gamma}(\text{pH}, \text{Mg}, \text{Ion})$, $P_{\alpha}(\text{pH}, \text{Mg}, \text{Ion})$, and $P_{\beta}(\text{pH}, \text{Mg}, \text{Ion})$ are calculated separately as described in Figure 2. The product of the three probability distributions, that is, $\prod_{i=\gamma,\alpha,\beta} P_i(\text{pH}, \text{Mg}, \text{Ion})$, yields the joint probability distribution $P_{\text{joint}}(\text{pH}, \text{Mg}, \text{Ion})$. The final output values pH_{Out} , Mg_{Out} , and Ion_{Out} are calculated as the weighted means of all possible values. Source: Figure is taken and adapted with permission from Reference 24.

The datasets from the lower leg muscles of healthy volunteers were acquired with a 3D ^{31}P MRSI sequence with a nominal spatial resolution of $(8 \times 8 \times 16) \text{ mm}^3$, $\alpha = 20^\circ$, $T_R = 240 \text{ ms}$, a spectral resolution of 4.88 Hz/point, and Hamming-weighted k-space acquisition with 16 averages in the k-space center. The total acquisition time was 56 min. Before quantification, all datasets were processed using onefold spatial zero-filling, and a 10 Hz Gaussian filter in the time domain.

The datasets from the patients with glioblastoma were acquired with a 3D ^{31}P MRSI sequence with a nominal spatial resolution of $(12.5 \times 12.5 \times 12.5) \text{ mm}^3$, $\alpha = 20^\circ$, $T_R = 250 \text{ ms}$, a spectral resolution of 4.88 Hz/point, Hamming-weighted k-space acquisition with 18 averages in the k-space center, and ^{31}P - ^1H nuclear Overhauser effect (NOE) enhancement. The total acquisition time was 51 min. Before quantification, all datasets were processed by low-rank filtering, onefold spatial zero-filling, and a 10 Hz Gaussian filter in the time domain.

Quantification of the ^{31}P spectra was performed using a custom-made implementation of the AMARES algorithm²³ for MATLAB.¹ The fit model included six resonance peaks, that is, PCr, the three resonances of ATP, P_i , and glycerophosphocholine (GPC) in the case of muscle datasets. In the case of brain data, the fit model additionally included phosphoethanolamine (PE), phosphocholine (PC), 2,3-diphosphoglycerate (DPG), extracellular P_i (eP_i), mobile phospholipids (MPLs), nicotinamide adenine dinucleotide (NAD(H)), and uridine diphosphoglucose (UDPG). For the full description of all acquisition parameters and quantification steps in case of muscle and brain datasets, the reader is referred to the work of Franke et al.²⁵ and Korzowski et al.,² respectively.

The quantified chemical shifts (δ_{γ} , δ_{α} , δ_{β}) from the in vivo datasets (all voxels within tissue masks without applying any rejection criteria regarding spectral or fitting quality) were fed voxelwise into the algorithm, yielding 3D maps for pH, Mg, and Ion. For the error margin, a Gaussian distribution with a width of $\sigma = 0.02 \text{ ppm}$ was assumed (compare Section 2.3 and Figure 2A). The choice of $\sigma = 0.02 \text{ ppm}$ was based on the approximated frequency precision of the used fitting model, that is, in the best case, a discrimination of neighboring spectral points (estimated as half of the spectral resolution) is possible. The same error margin was applied for all voxels. Note that other choices for the error margin are possible (cf. Section 4.3).

The shown maps for Mg are given as the total magnesium ion concentration relative to the total ATP concentration, that is, $R = [\text{Mg}^{2+}_{\text{total}}]/[\text{ATP}^{4-}_{\text{total}}]$. For the muscle datasets, $[\text{ATP}^{4-}_{\text{total}}] = 5 \text{ mM}$ is assumed,^{26,27} and for the brain datasets $[\text{ATP}^{4-}_{\text{total}}] = 3 \text{ mM}$.^{27,28} The resulting maps for pH_{Out} , R_{Out} , and Ion_{Out} are qualitatively compared with conventionally calculated maps for pH and the free magnesium ion concentration $[\text{Mg}^{2+}_{\text{free}}]$. To this end, for all used in vivo data sets, also pH maps are calculated by using the modified form of the Henderson–Hasselbalch equation employing the quantified chemical shift of P_i with constants from Reference 14. Maps showing the free magnesium ion concentration are calculated based on the formula given in References 16 and 29 using the chemical shift difference between the α - and β -resonances of ATP. These maps will be referred to as the conventional maps for pH and Mg, that is, pH_{Conv} and $[\text{Mg}^{2+}_{\text{free}}]_{\text{Conv}}$. It should be emphasized once again that pH_{Conv} is based on the chemical shift of P_i , and that this calculated pH value is also used for the calculation of $[\text{Mg}^{2+}_{\text{free}}]_{\text{Conv}}$ (compare Formulas 4–6 in Reference 29). Moreover, it should be noted that the implemented look-up algorithm aims at total Mg, whereas the calculated $[\text{Mg}^{2+}_{\text{free}}]_{\text{Conv}}$ maps show the free magnesium ion concentration.

3 | RESULTS

3.1 | Implementation of the look-up table and verification of the algorithm

The ^{31}P spectra acquired from the model solutions were of high quality, enabling a robust quantification of all metabolites contained in the solutions (Figure 4A,B), and thus enabling the extraction of 114 triples of measured ATP chemical shifts. With respect to the data acquired in vivo (Figure 4C,D), the individual chemical shifts are mostly captured by the sets of model solutions, except for the highest α -ATP chemical shifts observed in parts of the muscle data (maximum discrepancy $\sim 0.07 \text{ ppm}$, cf. Figure S3 in the Supporting Information).

The extension of the look-up table elements beyond the measured entries via inter- and extrapolation of the chemical shifts using the developed model functions $\delta_i^{\text{model}}(\text{pH}, \text{Mg}, \text{Ion})$, $i \in (\gamma, \alpha, \beta)$, was possible (adjusted $R^2 > 0.99$).

As a basic plausibility test of the implemented look-up algorithm, the measured ATP chemical shifts of the model solutions were assigned to (pH, Mg, Ion) using the interpolated look-up table. Figure 5 demonstrates the matched output parameters (pH_{Out} , Mg_{Out} , Ion_{Out}) compared with the prepared parameters for a representative set of model solutions. The measured deviations quantify the differences between model functions and measurements. The deviation between determined and prepared values is in general small for pH and magnesium, except for the model

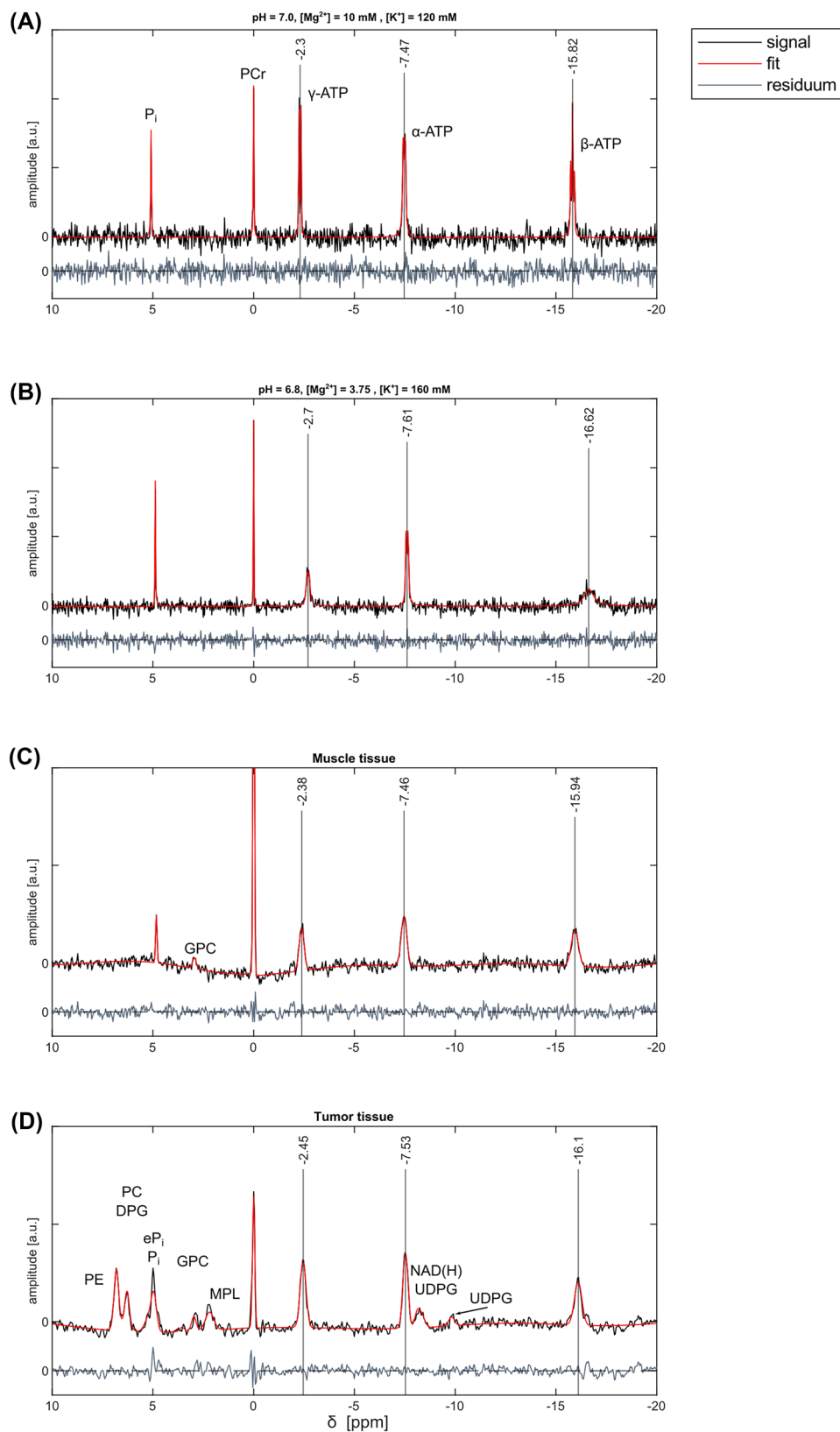


FIGURE 4 Legend on next page.

FIGURE 4 Representative ^{31}P spectra acquired in model solutions (A, B) and in vivo (C, D). A, B, The spectra from model solutions were acquired with a ^{31}P FID sequence at $B_0 = 9.4$ T. A robust quantification of all contained metabolites was possible: P_i , PCr , and ATP . The quantified chemical shifts of ATP , which are of relevance for the look-up table, are indicated in each spectrum. C, D, The representative in vivo spectra were acquired with a ^{31}P MRSI sequence at $B_0 = 7$ T. C, The spectrum from muscle tissue was obtained from the soleus muscle of a healthy volunteer. Here, also the resonance of GPC was observed. D, The spectrum from tumor tissue was obtained from a patient with glioblastoma. Here, also the resonances of PE , PC , DPG , eP_i , MPLs , NAD(H) , and UDPG are observed.

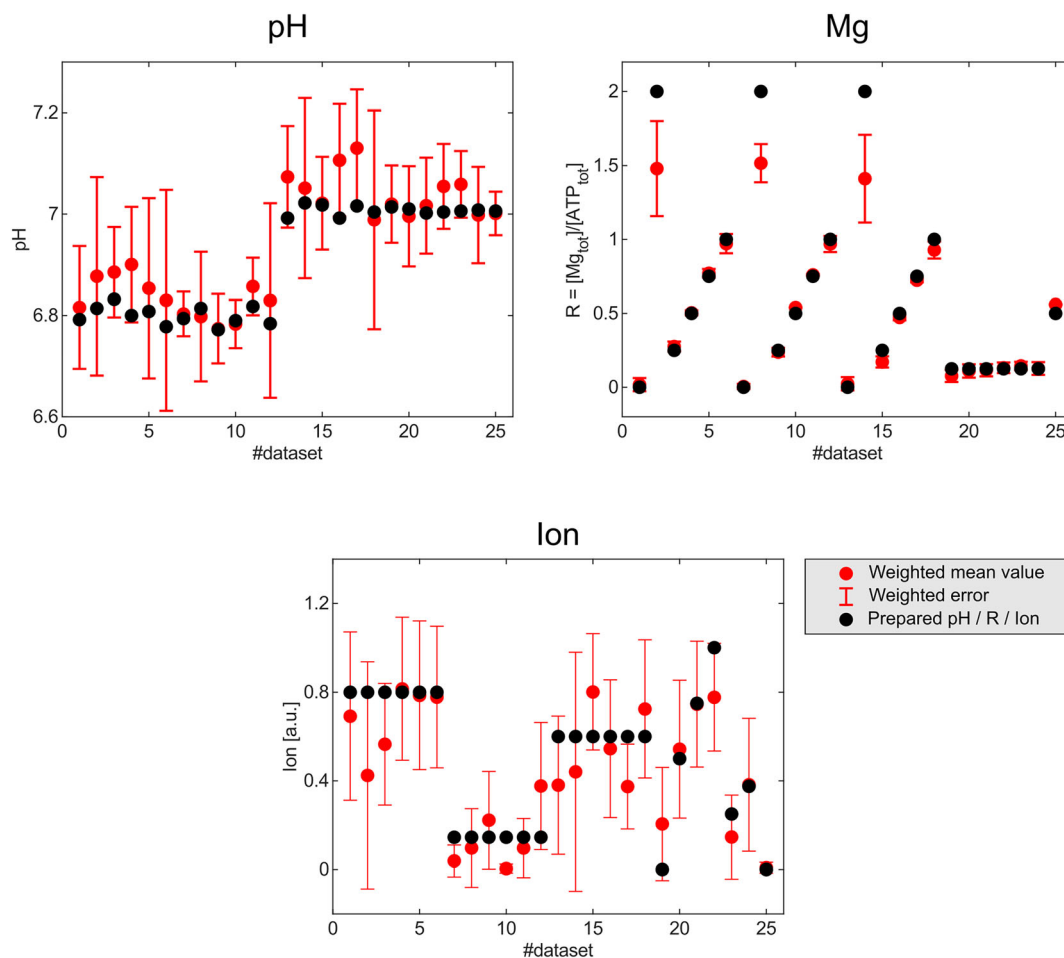


FIGURE 5 Results of a basic plausibility test of the implemented look-up algorithm. The measured ATP chemical shifts of a representative set of model solutions were assigned to $(\text{pH}, \text{Mg}, \text{Ion})$ using the interpolated look-up table. The matched output parameters (pH_{Out} , Mg_{Out} , Ion_{Out}) (red) are compared with the prepared parameters (black). Hereby, the weighted mean values and weighted errors as described in Section 2.3 are shown. The deviation between determined and prepared values is in general small for pH and Mg , except for the datasets with a high magnesium content, that is, $R = 2$. The deviation between determined and prepared values is the largest for the parameter Ion , but lies within the error margin for most of the shown datasets.

solutions with a high magnesium content, that is, $R = 2$. The deviation between determined and prepared values is the largest for the parameter Ion , but is still within the error margin for almost all datasets.

3.2 | Application of the implemented look-up algorithm to in vivo ^{31}P MRSI data

The application of the implemented look-up algorithm to in vivo ^{31}P MRSI data as described in Section 2.3 yielded a successful determination of solution triples (pH_{Out} , Mg_{Out} , Ion_{Out}) in only a small number of voxels. For the lower leg muscle data, a solution triple could be determined in only 18% of all muscle voxels. For the brain data sets, a solution triple was found in only 50% of the brain voxels. The failed assignment of solution triples was found to result from mismatches of the chemical shifts of $\alpha\text{-ATP}$, which will be discussed in Section 4.2. Therefore, the look-up algorithm

was reduced to the chemical shifts of only γ - and β -ATP, and applied to the in vivo data. With this reduced version of the algorithm, in 99% (muscle data) and 94% (brain data) of all tissue voxels plausible output values for (pH, Mg, Ion) could be determined. Representative slices of the resulting volumetric maps for pH_{Out} , R_{Out} and Ion_{Out} are shown in Rows 2–4 of Figures 6 and 7. The conventionally calculated maps for pH and $[\text{Mg}^{2+}_{\text{free}}]$ are shown in Rows 1 and 5 respectively.

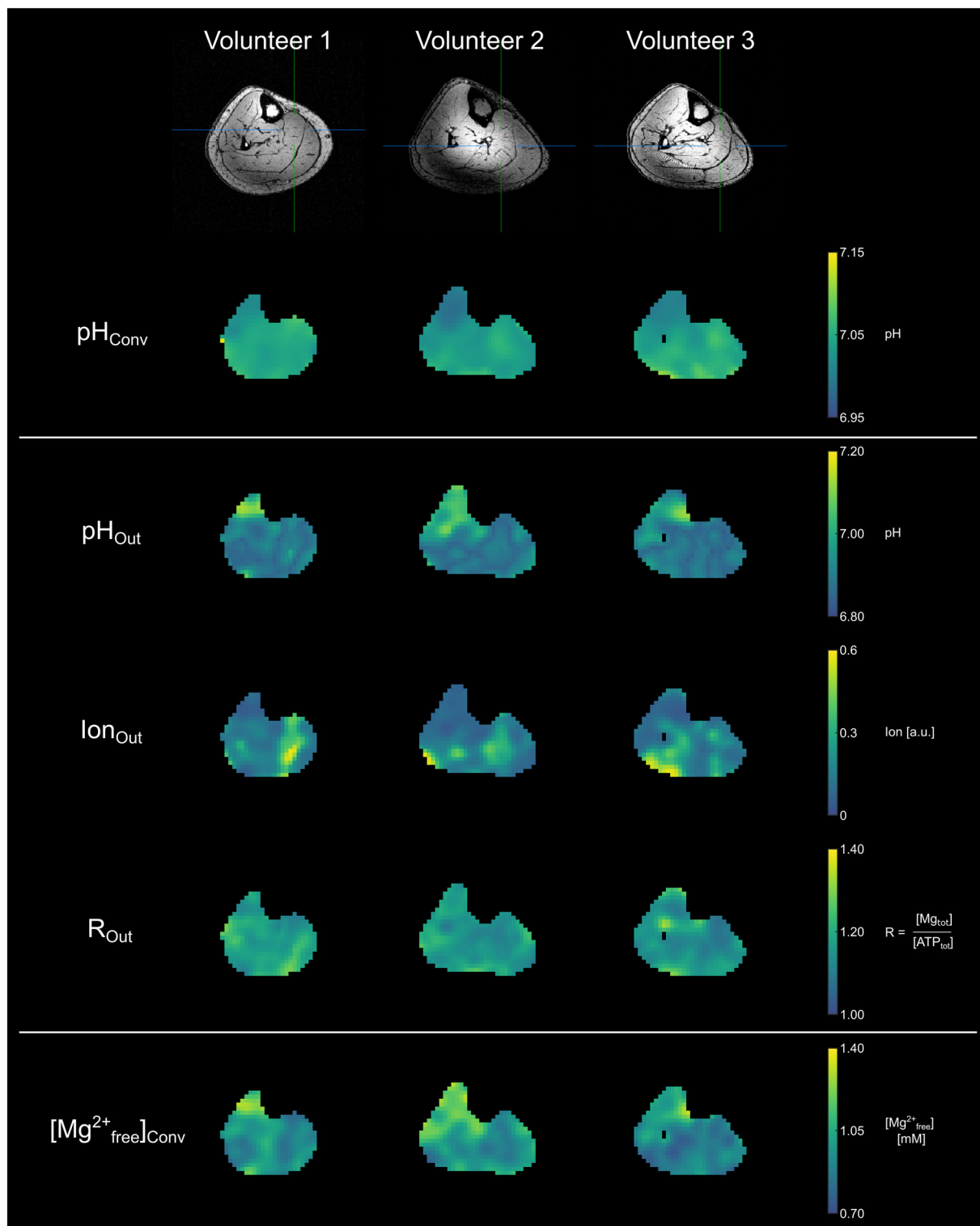


FIGURE 6 Transversal view of the 3D maps for pH_{Out} , Ion_{Out} , and R_{Out} resulting from the application of the implemented look-up algorithm to 3D MRSI datasets acquired in the lower leg muscles of three healthy volunteers. As described in Section 2.4, Mg is given as $R = [\text{Mg}_{\text{total}}]/[\text{ATP}_{\text{total}}]$ assuming $[\text{ATP}_{\text{total}}] = 5 \text{ mM}$ for the human leg muscle.^{26,27} In the first and last rows, the conventionally calculated maps for pH and the free magnesium ion concentration, that is, pH_{Conv} and $[\text{Mg}^{2+}_{\text{free}}]_{\text{Conv}}$, are also shown. Note the different value ranges.

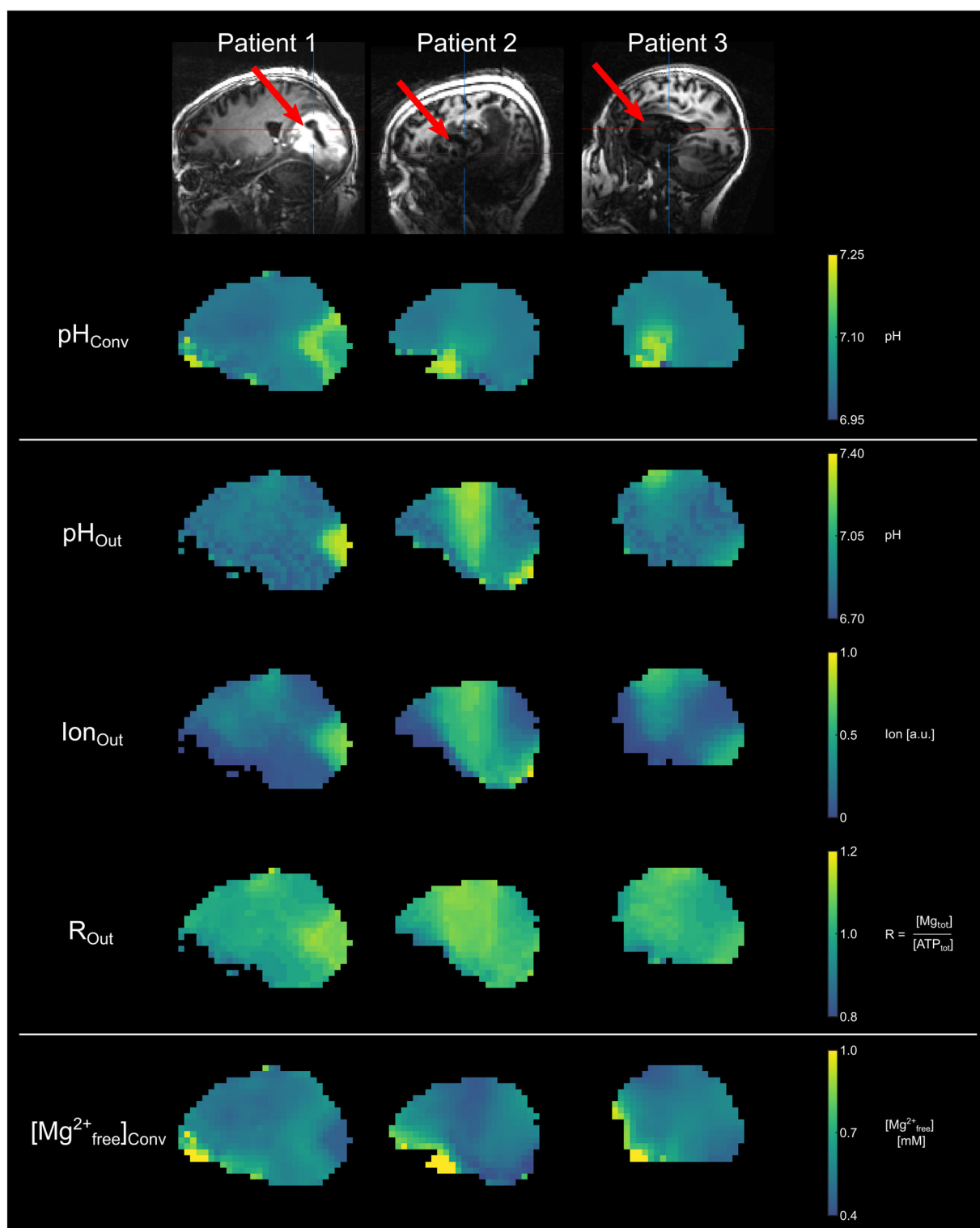


FIGURE 7 Sagittal view of the 3D maps pH_{Out} , Ion_{Out} , and R_{Out} resulting from the application of the implemented look-up algorithm to 3D MRSI datasets acquired in the brains of three patients with glioblastoma. The locations of the tumors are indicated with red arrows in the first row. As described in Section 2.4, Mg is given as $R = [\text{Mg}_{\text{total}}]/[\text{ATP}_{\text{total}}]$ assuming $[\text{ATP}_{\text{total}}] = 3 \text{ mM}$ for the human brain.^{27,28} In the first and last rows, the conventionally calculated maps for pH and the free magnesium ion concentration, that is, pH_{Conv} and $[\text{Mg}^{2+}_{\text{free}}]_{\text{Conv}}$, are also shown. Note the different value ranges.

The application of the reduced version of the implemented look-up algorithm to the lower leg muscle data sets resulted in plausible values for pH between 6.8 and 7.3, and for R of 1–1.5 (corresponding to a total magnesium ion concentration of 5.0–7.5 mM). Local differences of the determined values (pH_{Out} , Ion_{Out} , R_{Out}) are apparent in the maps, which show the same trends for all three volunteers: for example, slightly

higher pH values in the tibialis anterior muscle and higher Ion values in the soleus muscle (Figure 6, Rows 2–4). These observed patterns in the output maps are partly different from the patterns in the conventionally calculated maps for pH and the free magnesium ion concentration (cf. Figure 6, Rows 1 and 5). For example, in the pH_{Conv} maps, lower pH values are observed in the tibialis anterior muscle. Interestingly, the look-up-based pH_{Out} map seems to have a similar pattern to the $[\text{Mg}^{2+}_{\text{free}}]_{\text{Conv}}$ map, whereas the pH_{Conv} map seems to be resembled by the Ion_{Out} map.

The application of the reduced look-up algorithm to the brain datasets of patients with glioblastoma resulted in a larger range of pH values than for the muscle datasets, that is, 6.7–7.4. The value ranges for R_{Out} and Ion_{Out} are slightly different from the ranges in the muscle data, that is, higher Ion and lower R values. For Patient 1, pH values of up to 7.4 were found in the tumor compared with about 6.9 in healthy tissue (Figure 7, Row 2). The pH_{Out} map shows a stronger contrast than the pH_{Conv} map, where values of only up to 7.25 in the tumor were determined (Figure 7, Row 1). The Ion_{Out} and R_{Out} maps of Patient 1 show increased values in the depicted slice of the map (Figure 7, Rows 3 and 4). Also here, the patterns of the look-up-based output maps differ from the patterns of the conventionally calculated maps pH_{Conv} and $[\text{Mg}^{2+}_{\text{free}}]_{\text{Conv}}$. Compared with the datasets of the lower leg muscle, a larger inter-subject variation is observed.

4 | DISCUSSION

In this article, we have proposed an alternative to the conventional calibration equations for the determination of pH and Mg by means of ^{31}P MRS(I), aiming for a more complete description of tissue microenvironment: for example, accounting for varying ionic strength. The focus lay on two main aspects: (i) the introduction of the basic concept of mapping multiple dependences of ^{31}P spectral properties to biochemical parameters, and (ii) the implementation of a suitable look-up algorithm directly incorporating data imperfection. The proposed approach is well generalizable, and is extensible if novel data are available. Due to the incorporation of multiple parameters, the application of the proposed approach might generate novel knowledge about the tissue microenvironment in the future.

As a first demonstration of our look-up-approach *in vivo*, we used only the chemical shifts of ATP (in contrast to P_i and ATP in the conventional methods) to estimate pH and Mg values in different tissue types (healthy and diseased), potentially subject to different ionic conditions. While plausible pH and Mg maps could be generated, the *in vivo* application also unraveled potential for improvements and pitfalls.

4.1 | Comparison with other methods

It is well known that ^{31}P chemical shifts are affected by various parameters: for example, the pH value (exploited in the conventional Henderson–Hasselbalch-based approaches), the magnesium ion concentration, the overall ionic strength,^{30,31} or the temperature.³² Also the measured linewidths^{31,33} and the J-coupling constants^{34–37} of the ATP resonances are known to be influenced by changes of the magnesium ion concentration. Based on this knowledge, the idea of a multi-parametric look-up table, that is, to use multiple spectral parameters containing valuable information for the determination of pH and Mg, by means of ^{31}P MRS(I) is promising.

An approach for the simultaneous determination of pH and magnesium ion concentration comparable to our approach had already been proposed in the past.³⁸ However, a major difference in our approach is the inclusion of a further biochemical parameter, that is, the ionic strength. In contrast to Williams et al.,³⁸ who considered the ionic strength to be negligible for the determination of pH and magnesium ion content, we considered the ionic strength to have a substantial influence, especially when applied to pathologic conditions, where the ionic composition might change.^{39,40} A change in the ionic strength might alter equilibrium constants (for example, pK_A and K_D), affecting the estimation of pH and magnesium ion content.

In this regard, another difference from the existing methods based on calibration equations becomes apparent. In the conventional modified Henderson–Hasselbalch equation, for example, a stable modeling of the calibration curve (relating the measured chemical shift to pH) in terms of accurate determination of the needed constants (which depend on the ionic strength) requires data sampling also at pH values irrelevant under *in vivo* conditions. The acquisition of multiple calibration curves valid for different ionic conditions, that is, varying pK_A of different tissues, consequently might result in inefficient data sampling (e.g., repetitive sampling of irrelevant pH values). In contrast, in our approach, the direct mapping of multiple spectral properties to multiple biochemical parameters, also including a measure for the ionic strength, allows for a more efficient data sampling. This, in principle, enables us to focus more on data points that are relevant *in vivo*, that is, a more efficient sampling of assumed pH ranges, and ultimately to increase the dimensionality of the sampled parameter space (e.g., different ionic constituents).

Even more importantly, the particular strength of the approach proposed herein is the inclusion of uncertainty margins on the measured chemical shifts in the implemented algorithm, which increases the robustness of the estimation of pH and Mg. Furthermore, this means that intrinsically imperfect data quality (both in the model solution datasets used for generation of the look-up table and in the *in vivo* data) are reasonably accounted for, because the algorithm directly considers a specific error margin.

4.2 | Generation of look-up table and performance of the algorithm

The most crucial aspect for an application of the proposed method in vivo is the assumption that the generated entries of the look-up table sufficiently reflect in vivo conditions. Although the proposed approach incorporates additional biochemical parameters, that is, changing ionic strength, discrepancies between the prepared model solutions and in vivo conditions still exist. Factors that lead to a discrepancy between model solutions and in vivo measurements include (i) the temperature of the model solution during the measurement and during the sample preparation, (ii) the chemical composition of the prepared model solutions (i.e., other relevant ions not included so far, interaction with proteins, buffer solution used). Although optimization of the model solution composition is possible, mimicking the true in vivo conditions remains challenging. A potential benefit of the proposed look-up algorithm regarding the missing knowledge about the exact conditions in vivo is that unestimated parameters act as nuisances and thus are captured as additional uncertainty.

Note that, although our approach is more efficient in generation of relevant data points compared with the conventional methods, the generation process is still challenging (so far only 114 consistent chemical shift triples have been generated). To virtually improve the coverage of the target parameter space, and thus increase the resolution of the assignment of output values, a model was still used. The developed model, which is based on the Hill equation, has only a weak dependence on changes of the parameter Ion , which leads to a smoothing of the true dependence observed in the acquired data. This smoothing of the Ion dependence due to the model function poses a problem for the determination of the parameter Ion . Further, note that other uncaptured contributions existing in vivo might also be incompatible with the applied model, highlighting the need to remove the modeling step in the future. In this regard, another benefit of our approach is that the look-up table can be updated continuously, when novel model solutions are prepared and measured. In the future, the currently interpolated look-up table entries could potentially be replaced by actually acquired data points, thus approaching a “true look-up table”.

Before applying the implemented look-up algorithm to in vivo ^{31}P MRSI data, a basic plausibility test was performed by matching the quantified ATP chemical shifts of the model solutions to the parameters (pH_{Out} , Mg_{Out} , Ion_{Out}). This basic plausibility test showed that, in principle, the algorithm works as intended, that is, assigns plausible output values to the input triples. Note that so far the same datasets have been used for both the development of the model functions $\delta^{\text{model}}(\text{pH}, \text{Mg}, \text{Ion})$ and as test data sets for the plausibility test. In the future, independent model solutions should be prepared in order to have a separate set of test data for a more meaningful plausibility test, which could presumably allow for a better analysis of the algorithm's performance. However, so far, we have limited this plausibility test to the already existing datasets, since the focus of this work is the application in vivo.

The application of the developed look-up algorithm using all three ATP chemical shifts (as described in Section 2) to the in vivo data was possible only in some of the voxels, as already mentioned in Section 3.2. Analyses revealed that the failing assignment of joint solution triples was due to the solution triples determined based on the chemical shift of $\alpha\text{-ATP}$. Either the input value, that is, the measured chemical shift in vivo $\delta_{\alpha}^{\text{meas}}$, was not represented in the entries of the look-up table (hence no assignment was possible; maximal discrepancy of ~ 0.07 ppm, cf. Supporting Information S3), or the possible solution triples based on δ_{α} , that is, $(\text{pH}, \text{Mg}, \text{Ion})_{\alpha}$, differed from the possible solution triples based on δ_{γ} and δ_{β} , that is, $(\text{pH}, \text{Mg}, \text{Ion})_{\gamma}$ and $(\text{pH}, \text{Mg}, \text{Ion})_{\beta}$.

In this context, we found it unexpected, that the range of $\alpha\text{-ATP}$ chemical shifts (in reference to PCr) measured in vivo was relatively large (between -7.38 and -7.70 ppm; cf. Supporting Information S3), although δ_{α} is less sensitive to variations in biochemical parameters than δ_{γ} and δ_{β} . Moreover, the highest δ_{α} in muscle tissue could not be realized in our model solutions, even for the highest Mg concentrations considered (cf. Supporting information S3). Interestingly, the chemical shift differences of the ATP resonances relative to each other, that is, $\delta_{\gamma\alpha}$, $\delta_{\alpha\beta}$, and $\delta_{\gamma\beta}$, measured in our model solutions are in good agreement with earlier studies on model solutions with comparable chemical compositions (e.g., limiting chemical shifts $\delta_{\alpha\beta}^{\text{MgATP}} = 8.25$ ppm and $\delta_{\alpha\beta}^{\text{ATP}} = 10.80$ ppm from References 34 and 38 compared with a $\delta_{\alpha\beta}$ range of 8.28–11.10 ppm acquired in our model solutions). This might be a hint that the failing assignment is not directly related to the ATP chemical shifts obtained in our model solutions, and more importantly, that we did not miss a contribution solely affecting δ_{α} in a substantial manner, this being unlikely in any case. Thus, in principle, a look-up table employing only the chemical shift differences $\delta_{\gamma\alpha}$, $\delta_{\alpha\beta}$, and $\delta_{\gamma\beta}$ could improve the rate of successful assignments. However, such a look-up table would constitute only two non-redundant chemical shift differences ($\delta_{\gamma\alpha} + \delta_{\alpha\beta} = \delta_{\gamma\beta}$), thus there might be ambiguities if targeting the assignment of three parameters (pH, Mg, Ion). For this reason, we initially decided to use the three chemical shift differences of ATP (δ_{α} , δ_{γ} , δ_{β}) relative to PCr, in order to introduce a further non-redundant parameter. One might speculate that this very referencing is the problem, as PCr is assumed to be always at 0 ppm in our analyses, but can be also affected by varying biochemical parameters to a certain extent. Indeed, the discrepancy of about 0.07 ppm for δ_{α} between look-up table and in vivo data (cf. Section 3.1), as well as the unexpected large range of $\alpha\text{-ATP}$ chemical shifts in vivo of approximately 0.4 ppm, could be also induced by a change of PCr chemical shifts in different tissue types. Note that this would correspond to a bulk shift of ATP resonances, which would affect also the estimated pH and Mg values by assigning different entries of the look-up table. Thus, it is not surprising that the look-up algorithm finally applied in vivo employing only δ_{γ} and δ_{β} (being also potentially subject to ambiguities), is working, because the rather small bulk shifts are compensated by the stronger Mg and pH dependences on these chemical shifts.

To investigate the reasons for the failing assignments using all three ATP chemical shifts, and hence to improve the reliability of the value assignment by implementing an updated version of the look-up algorithm, there are the following possibilities: (i) testing of another chemical shift

reference, that is, use of relative chemical shift differences instead of all referencing to PCr, (ii) identifying the cause of the bulk shift, and (iii) alternatively, another spectral property could be incorporated as surrogate for a third parameter.

4.3 | Application of the implemented approach to in vivo data

The rationale for the development of the presented approach was to increase the reliability of the estimation of pH and Mg under changing biochemical conditions. It is reasonable to speculate that different tissues have—to a certain extent—different ionic compositions because of their various functions. In tumor tissue in particular it is known that ion concentrations are heavily altered.³⁹ There, significant ionic changes could influence the individual chemical shifts or calibration conditions in Henderson–Hasselbalch type calculations.

In the conventional calibration equations, the validity of the required constants, that is, apparent pK_A and K_D are assumed to be general, and thus also applicable in diseased tissue. However, a change of the chemical shift of P_i for example could also be induced by a change of the pK_A value of P_i (altering the chemical equilibrium conditions at constant pH) instead of a change in pH (interchangeability of pH and pK_A in the modified Henderson–Hasselbalch equation). Supporting this point, in fact, the parameters pH_{Conv} and Ion_{Out} seem to be interchangeable in Figures 6 and 7, that is, show similar morphological patterns. The same holds true for K_D : that is, a change in K_D due to a change in ionic strength would alter the determined magnesium concentration.

Because the α -ATP shift could not be employed for the in vivo data, the results demonstrated in Figures 6 and 7 are potentially subject to ambiguities, that is, three parameters (pH, Mg, Ion) are determined by the use of only two input parameters (δ_γ , δ_β). Nevertheless, the values obtained in vivo prove plausible, particularly the increased pH values obtained in tumor tissue of all patients, being qualitatively in agreement with earlier studies.^{1,4,41} Interestingly, the ionic strength, also including Mg as specific contributor, is increasing, which agrees with Taylor et al.,³ who obtained increased free magnesium ion to free ATP ratios in brain tumors compared with surrounding healthy tissue.

Note that, due to voxel bleed, spectral signatures from muscle tissue might contaminate the results in brain tissue (cf. Patient 2 in Figure 7), and that in the Mg maps a change of ATP concentration has additionally to be considered for a fair comparison.

Furthermore, it is worth highlighting that the use of the ATP chemical shifts only (instead of P_i in the case of the conventional pH determination method) can be beneficial in terms of (i) quantification reliability of the required resonance peaks in pathologic tissue (e.g., cancer), where a clear separation of different P_i compartments might be challenging due to the hypothesized opposing trends of intra- and extracellular pH leading to an overlap of different P_i resonance peaks,¹ and (ii) a possibly higher signal-to-noise ratio (SNR) in some tissues, potentially allowing for a reduction in measurement time (when sequence parameters, i.e., flip angle and T_R , are optimized for ATP signals). Nevertheless, in situations where the P_i resonance is well resolved and already of high SNR (e.g., in the muscle data shown in Figure 4C), the application of a look-up algorithm also incorporating P_i might improve the estimation of output values, and potentially solve the assignment problem caused by the α -ATP mismatch.

Finally, we want to briefly discuss our choice for the chemical shift error margin fed into the look-up algorithm. In this first implementation of the proposed algorithm, we have assumed a fixed global error margin for all voxels and for all input chemical shifts. This error margin is a pre-defined chemical shift range, which is Gaussian weighted with a specific width σ . In contrast to a global error margin for all resonances, a specific value for the error margin tailored to the individual voxel and individual resonance (i.e., γ -, α -, β -ATP) would be possible. One viable alternative for the weighted chemical shift range would be the use of the specific resonance linewidth quantified for each voxel and each resonance peak individually. Therewith, also the influence of the B_0 field homogeneity could be addressed and incorporated into the pH and Mg determination (cf. overview of PCr linewidths measured in vivo, shown in Supporting Information S5). Alternatively one could consider using the Cramér–Rao lower bounds (CRLBs) of the quantified chemical shifts. However, further analyses of these alternatives have to be performed in order to prove a benefit of such local error margins.

Altogether, the application of our proposed approach to in vivo conditions appears promising, and should be further developed. In general, the implemented look-up algorithm—in its current form—is in principle independent of the field strength at which the input data are acquired, because the only input parameters are the ATP chemical shifts (relative to PCr). As long as the ATP chemical shifts can be acquired reliably enough (e.g., without any overlap with other resonances), the proposed method is also applicable at lower field strengths (e.g., 1.5 or 3 T).

4.4 | Outlook

Future work should focus on a refinement of the acquired look-up table in order to enable a more reliable determination of biochemical parameters based on acquired ^{31}P spectral properties. This can be achieved either by adding more data points to the look-up table and/or by including additional dimensions.

Moreover, it is important to investigate the mismatch between the chemical shifts measured in vivo and in the prepared model solutions. As mentioned above, the influence of other ions, for example, sodium or calcium, should be investigated. Besides other ions, also the influence of the temperature during acquisition and during titration should be considered again, potentially helping to better capture in vivo spectral signatures.

Finally, cross-validation of results obtained by ^{31}P MRS with other non-MR-based modalities able to determine pH and Mg in vivo (e.g., PET-based pH probes,⁴² Mg binding fluorescent indicators⁴³) would be an important step towards improving the reliability of the proposed method. A major point of future work, which might also reveal new insights, should be the extension of the look-up table by including additional spectral parameters. In particular, the linewidths of the ATP resonances are interesting parameters, as they show a strong dependence on the Mg/ATP ratio. Therewith, the determination of Mg could become more robust, which furthermore could improve the determination of the other two parameters pH and Ion (as more data are gathered and can be combined, thus limiting the possible solution triples). Note that an incorporation of linewidths as parameters in the look-up table requires more careful consideration of the “calibration field strength” (i.e., acquisition of look-up table elements at 9.4 T) and the “measurement field strength” (i.e., measurements of in vivo data at 7 T), since relaxation properties will differ and the exchange regime relevant for the Mg-ATP complex might change.

Besides this, the parameter Ion (used as an overall measure for changes in the ionic composition) could be disentangled in the future, that is, considering each ionic contribution as a separate parameter, potentially allowing for a more profound tissue characterization.

Furthermore, the implemented multi-parametric look-up table is suited for the application of machine learning algorithms, when more data points will be acquired in the future. As an alternative to the current model-based search algorithm (cf. Section 2.3), one could consider implementing a machine-learning-based algorithm, for example, a random forest regression or gradient boosting regression.

5 | CONCLUSION

In this article, we have proposed a multi-parametric look-up algorithm aiming at the condition-independent estimation of the pH value and the magnesium ion content by means of ^{31}P MRS(I). Based on probability functions incorporating specific measurement uncertainties, the proposed algorithm enables the assignment of multiple measured spectral properties to the most plausible biochemical parameters defined in a pre-generated look-up table. As proof of concept, we applied a look-up algorithm employing only the chemical shifts of γ - and β -ATP to in vivo ^{31}P MRSI data in order to generate volumetric maps visualizing pH and magnesium ion content. For a more reliable determination of the biochemical parameters, the proposed look-up approach can be extended in the future by including additional quantifiable parameters of a ^{31}P spectrum. This might enable a more profound tissue characterization, being particularly of interest for application to pathologies, where multiple biochemical parameters may be altered to an extent not yet known.

ACKNOWLEDGEMENTS

Open Access funding enabled and organized by Projekt DEAL.

DATA AVAILABILITY STATEMENT

The code that support the findings of this study are openly available under <http://doi.org/10.5281/zenodo.10519157>. The data that support the findings of this study are available from the corresponding author upon request.

ORCID

Vanessa L. Franke  <https://orcid.org/0000-0002-2443-8352>

Johannes Breitling  <https://orcid.org/0000-0001-8003-5382>

Philip S. Boyd  <https://orcid.org/0000-0002-5914-2535>

Heinz-Peter Schlemmer  <https://orcid.org/0000-0002-9291-0954>

Mark E. Ladd  <https://orcid.org/0000-0002-4128-9440>

Daniel Paech  <https://orcid.org/0000-0001-5755-6833>

Andreas Korzowski  <https://orcid.org/0000-0002-0244-9712>

REFERENCES

1. Korzowski A, Weinfurter N, Mueller S, et al. Volumetric mapping of intra- and extracellular pH in the human brain using ^{31}P MRSI at 7T. *Magn Reson Med*. 2020;84(4):1707-1723. doi:[10.1002/mrm.28255](https://doi.org/10.1002/mrm.28255)
2. Korzowski A, Weckesser N, Franke VL, et al. Mapping an extended metabolic profile of gliomas using high-resolution ^{31}P MRSI at 7T. *Front Neurol*. 2021;12:735071. doi:[10.3389/fneur.2021.735071](https://doi.org/10.3389/fneur.2021.735071)
3. Taylor JS, Vigneron DB, Murphy-Boesch J, et al. Free magnesium levels in normal human brain and brain tumors: ^{31}P chemical-shift imaging measurements at 1.5 T. *Proc Natl Acad Sci U S A*. 1991;88(15):6810-6814. doi:[10.1073/pnas.88.15.6810](https://doi.org/10.1073/pnas.88.15.6810)
4. Wenger KJ, Hattingen E, Franz K, Steinbach JP, Bähr O, Pilatus U. Intracellular pH measured by ^{31}P -MR-spectroscopy might predict site of progression in recurrent glioblastoma under antiangiogenic therapy. *J Magn Reson Imaging*. 2017;46(4):1200-1208. doi:[10.1002/jmri.25619](https://doi.org/10.1002/jmri.25619)
5. Klomp DWJ, van de Bank BL, Raaijmakers A, et al. ^{31}P MRSI and ^1H MRS at 7 T: initial results in human breast cancer. *NMR Biomed*. 2011;24(10):1337-1342. doi:[10.1002/nbm.1696](https://doi.org/10.1002/nbm.1696)

6. Paech D, Weckesser N, Franke VL, et al. Whole-brain intracellular pH mapping of gliomas using high-resolution ^{31}P MR spectroscopic imaging at 7 T. *Radiol Imaging Cancer*. 2024;6(1):e220127. doi:10.1148/rycan.220127
7. Resnick LM, Altura BT, Gupta RK, Laragh JH, Alderman MH, Altura BM. Intracellular and extracellular magnesium depletion in type 2 (non-insulin-dependent) diabetes mellitus. *Diabetologia*. 1993;36(8):767-770. doi:10.1007/BF00401149
8. Reyngoudt H, Lopez Kolkovsky AL, Carlier PG. Free intramuscular Mg^{2+} concentration calculated using both ^{31}P and ^1H NMRS-based pH in the skeletal muscle of Duchenne muscular dystrophy patients. *NMR Biomed*. 2019;32(9):e4115. doi:10.1002/nbm.4115
9. Kato T, Murashita J, Kamiya A, Shioiri T, Kato N, Inubushi T. Decreased brain intracellular pH measured by ^{31}P -MRS in bipolar disorder: a confirmation in drug-free patients and correlation with white matter hyperintensity. *Eur Arch Psychiatry Clin Neurosci*. 1998;248(6):301-306. doi:10.1007/s004060050054
10. Hamakawa H, Murashita JUN, Yamada N, Inubushi T, Kato N, Kato T. Reduced intracellular pH in the basal ganglia and whole brain measured by ^{31}P -MRS in bipolar disorder. *Psychiatry Clin Neurosci*. 2004;58(1):82-88. doi:10.1111/j.1440-1819.2004.01197.x
11. Chaumeil MM, Valette J, Baligand C, et al. pH as a biomarker of neurodegeneration in Huntington's disease: a translational rodent-human MRS study. *J Cereb Blood Flow Metab*. 2012;32(5):771-779. doi:10.1038/jcbfm.2012.15
12. Barbagallo M, Belvedere M, di Bella G, Dominguez LJ. Altered ionized magnesium levels in mild-to-moderate alzheimer's disease. *Magnes Res*. 2011;24(3):115-121. doi:10.1684/mrh.2011.0287
13. Moon RB, Richards JH. Determination of intracellular pH by ^{31}P magnetic resonance. *J Biol Chem*. 1973;248(20):7276-7278. doi:10.1016/S0021-9258(19)43389-9
14. De Graaf RA. *In Vivo NMR Spectroscopy: Principles and Techniques*. Wiley; 2013.
15. Gupta RK, Benovic JL, Rose ZB. The determination of the free magnesium level in the human red blood cell by ^{31}P NMR. *J Biol Chem*. 1978;253(17):6172-6176. doi:10.1016/S0021-9258(17)34595-7
16. Golding EM, Golding RM. Interpretation of ^{31}P MRS spectra in determining intracellular free magnesium and potassium ion concentrations. *Magn Reson Med*. 1995;33(4):467-474. doi:10.1002/mrm.1910330403
17. Meyerspeer M, Boesch C, Cameron D, et al. ^{31}P magnetic resonance spectroscopy in skeletal muscle: experts' consensus recommendations. *NMR Biomed*. 2021;34(5):e4246. doi:10.1002/nbm.4246
18. Petroff OA, Prichard JW, Behar KL, Alger JR, den Hollander JA, Shulman RG. Cerebral intracellular pH by ^{31}P nuclear magnetic resonance spectroscopy. *Neurology*. 1985;35(6):781-788. doi:10.1212/wnl.35.6.781
19. Pettegrew JW, Withers G, Panchalingam K, Post JFM. Considerations for brain pH assessment by ^{31}P NMR. *Magn Reson Imaging*. 1988;6(2):135-142. doi:10.1016/0730-725X(88)90443-2
20. Roberts JKM, Wade-Jardetzky N, Jardetzky O. Intracellular pH measurements by ^{31}P nuclear magnetic resonance. Influence of factors other than pH on ^{31}P chemical shifts. *Biochemistry*. 1981;20(19):5389-5394. doi:10.1021/bi00522a006
21. Madden A, Leach MO, Sharp JC, Collins DJ, Easton D. A quantitative analysis of the accuracy of in vivo pH measurements with ^{31}P NMR spectroscopy: assessment of pH measurement methodology. *NMR Biomed*. 1991;4(1):1-11. doi:10.1002/nbm.1940040102
22. White KA, Grillo-Hill BK, Barber DL. Cancer cell behaviors mediated by dysregulated pH dynamics at a glance. *J Cell Sci*. 2017;130(4):663-669. doi:10.1242/jcs.195297
23. Vanhamme L, Van Huffel S. AMARES: advanced method for accurate, robust and efficient spectral fitting of MRS data with use of prior knowledge. *J Magn Reson*. 1997;129:35-43. doi:10.1006/jmre.1997.1244
24. Franke VL. In vivo determination of pH and magnesium ion concentration by means of ^{31}P MRSI: a multi-parametric look-up approach—heiDOK. 2023. Accessed May 25, 2023. <https://archiv.ub.uni-heidelberg.de/volltextserver/32909/>
25. Franke VL, Breitling J, Ladd ME, Bachert P, Korzowski A. ^{31}P MRSI at 7 T enables high-resolution volumetric mapping of the intracellular magnesium ion content in human lower leg muscles. *Magn Reson Med*. 2022;88(2):511-523. doi:10.1002/mrm.29231
26. Schmidt RF, Lang F, Heckmann M. *Physiologie des Menschen: Mit Pathophysiologie*. Springer; 2010. doi:10.1007/978-3-642-01651-6
27. Greiner JV, Glonek T. Intracellular ATP concentration and implication for cellular evolution. *Biology*. 2021;10(11):1166.
28. Ren J, Sherry AD, Malloy CR. ^{31}P -MRS of healthy human brain: ATP synthesis, metabolite concentrations, pH, and T_1 relaxation times. *NMR Biomed*. 2015;28(11):1455-1462. doi:10.1002/nbm.3384
29. Barker PB, Butterworth EJ, Boska MD, Nelson J, Welch KMA. Magnesium and pH imaging of the human brain at 3.0 Tesla. *Magn Reson Med*. 1999;41(2):400-406. doi:10.1002/(SICI)1522-2594(199902)41:2<30.CO;2-E
30. Mosher TJ, Williams GD, Doumen C, Lanoue KF, Smith MB. Error in the calibration of the MgATP chemical-shift limit: effects on the determination of free magnesium by ^{31}P NMR spectroscopy. *Magn Reson Med*. 1992;24(1):163-169. doi:10.1002/mrm.1910240117
31. Mottet I, Demeure R, Gallez B, Grandin C, Van Beers BE, Pringot J. Experimental ^{31}P NMR study of the influence of ionic strength on the apparent dissociation constant of MgATP. *Magn Reson Mater Phys Biol Med*. 1994;2(2):101-107. doi:10.1007/BF01753065
32. Widmaier S, Hoess T, Breuer J, Jung WI, Dietze GJ, Lutz O. Magnesium-based temperature dependence of the ATP chemical-shift separation δ_{ATP} and its relation to intracellular free magnesium. *J Magn Reson B*. 1996;113(1):16-24. doi:10.1006/jmrb.1996.0150
33. Pecoraro VL, Hermes JD, Cleland WW. Stability constants of Mg^{2+} and Cd^{2+} complexes of adenine nucleotides and thionucleotides and rate constants for formation and dissociation of MgATP and MgADP. *Biochemistry*. 1984;23(22):5262-5271. doi:10.1021/bi00317a026
34. Widmaier S, Hoess T, Jung WI, Staubert A, Dietze GF, Lutz O. ^{31}P NMR studies of human soleus and gastrocnemius show differences in the J_{ATP} coupling constant of ATP and in intracellular free magnesium. *Magn Reson Mater Phys Biol Med*. 1996;4(1):47-53. doi:10.1007/BF01759779
35. Jung W, Staubert A, Widmaier S, et al. Phosphorus J-coupling constants. *Magn Reson Med*. 1997;37(5):802-804. doi:10.1002/mrm.1910370525
36. Son T-D, Roux M, Ellenberger M. Interaction of Mg^{2+} ions with nucleoside triphosphates by phosphorus magnetic resonance spectroscopy. *Nucleic Acids Res*. 1975;2(7):1101-1110. doi:10.1093/nar/2.7.1101
37. Mitsumori F. Phosphorus-31 nuclear magnetic resonance studies on intact erythrocytes. Determination of intracellular pH and time course changes in phosphorus metabolites. *J Biochem*. 1985;97(6):1551-1560. doi:10.1093/oxfordjournals.jbchem.a135212
38. Williams GD, Mosher TJ, Smith MB. Simultaneous determination of intracellular magnesium and pH from the three ^{31}P NMR chemical shifts of ATP. *Anal Biochem*. 1993;214(2):458-467. doi:10.1006/ABIO.1993.1523
39. Regnery S, Behl NGR, Platt T, et al. Ultra-high-field sodium MRI as biomarker for tumor extent, grade and IDH mutation status in glioma patients. *NeuroImage Clin*. 2020;28:102427. doi:10.1016/j.nicl.2020.102427

40. Müller HP, Nagel AM, Keidel F, et al. Relaxation-weighted ^{23}Na magnetic resonance imaging maps regional patterns of abnormal sodium concentrations in amyotrophic lateral sclerosis. *Ther Adv Chronic Dis*. 2022;13. doi:[10.1177/20406223221109480](https://doi.org/10.1177/20406223221109480)
41. Maintz D, Heindel W, Kugel H, Jaeger R, Lackner KJ. Phosphorus-31 MR spectroscopy of normal adult human brain and brain tumours. *NMR Biomed*. 2002;15(1):18-27. doi:[10.1002/NBM.735](https://doi.org/10.1002/NBM.735)
42. Chen LQ, Pagel MD. Evaluating pH in the extracellular tumor microenvironment using CEST MRI and other imaging methods. *Adv Radiol*. 2015;2015:206405. doi:[10.1155/2015/206405](https://doi.org/10.1155/2015/206405)
43. Günther T. Concentration, compartmentation and metabolic function of intracellular free Mg^{2+} . *Magnes Res*. 2006;19(4):225-236. doi:[10.1684/mrh.2006.0067](https://doi.org/10.1684/mrh.2006.0067)

SUPPORTING INFORMATION

Additional supporting information can be found online in the Supporting Information section at the end of this article.

How to cite this article: Franke VL, Breitling J, Boyd PS, et al. A versatile look-up algorithm for mapping pH values and magnesium ion content using ^{31}P MRSI. *NMR in Biomedicine*. 2024;37(6):e5113. doi:[10.1002/nbm.5113](https://doi.org/10.1002/nbm.5113)